The International Journal of Advanced Manufacturing Technology (2024) 134:1699–1710
https://doi.org/10.1007/s00170-024-13915-y

ORIGINAL RESEARCH

Establishment of CFRP drilling simulation model considering heat accumulation effect and study on its delamination damage

Yiwei Zhang[1,2] · Zhiwei Hu[2,3] · Guixing Wang[2,4] · Lifeng Wang[1] · Qiang Luo[1]

Received: 9 November 2023 / Accepted: 26 May 2024 / Published online: 7 August 2024

Abstract

The utilization of carbon fiber-reinforced polymer/plastic (CFRP) components is primarily limited due to the lack of high-quality and least damage-based hole constructing technology. In this study, the delamination defect is investigated at the exit of CFRP drilling by a novel three-dimensional simulation model considering heat accumulation effect. The validity of the model is confirmed through experimental data of CFRP boreholes: surface temperature distribution at the borehole outlet, drilling axial force, and delamination factor at the outlet. The model exhibited high accuracy in theoretical analysis of CFRP 3D drilling with/without temperature. Additionally, the variation in temperature field and corresponding delamination damage is analyzed through simulation of CFRP drilling process at the exit plane of a hole. Results indicate that delamination damage occurs during unsupported dry drilling when half of the length of the main cutting edge impale the workpiece after reaching its exit plane. The changes in axial force caused delamination under different processing parameters, and a quantitative relationship is established through multiple regression analysis. The appropriate processing parameters can effectively reduce delamination during CFRP drilling. Specifically, accurate measures can ensure sufficient heat conduction and minimize heat accumulation during the formation stages of exit-related delamination.

Keywords CFRP drilling · Delamination damage · Heat accumulation effect · Simulation model

1 Introduction

The carbon fiber-reinforced polymer (CFRP) refers to a novel class of composite materials. Carbon fibers embedded in an epoxy matrix enable a lightweight nature with high strength, corrosion resistance, and fatigue endurance [1]. Diverse industrial sectors including aerospace, shipbuilding, and automotive use CFRP components, which are integrated and manufactured through laying and curing processes. For component connection and assembly, the connection holes are required. However, the processing quality of connection holes can affect the strength, stiffness, and reliability of the components. The delamination, tearing, burrs, and other damages caused by CFRP drilling can compromise the load-bearing capacity, as per statistical data. Importantly, the delamination can reduce 10–70% of bearing capacity [2, 3]. At present, traditional spiral milling and drilling in addition to water jet, laser, and electric spark can create CFRP hole [4–7]. The CFRP components require minimum-loss and high-quality connection holes applicability in aerospace. It demands traditional drilling with good universality and strong controllability [8].

The research focus of CFRP drilling holes is the inhibition of processing damage such as tearing, burr, and delamination [9]. Dipaol et al. [10] conducted an experimental study on tear propagation during unidirectional CFRP drilling. They believed that the initial crack of the workpiece was not necessarily within the hole radius due to the influence of processing technology and hole-forming geometry and proposed that the root cause of delamination diffusion was the expansion of laminates, opening spalling, and opening tearing/torsion. Jain et al. studied the drilling process of CFRP with a twist drill and

✉ Yiwei Zhang
ywzhang@sanxiau.edu.cn

1 School of Mechanical Engineering, Chongqing Three Gorges University, Chongqing, China

2 School of Mechatronic Engineering, Southwest Petroleum University, Chengdu, China

3 CRRC Meishan Co., Ltd, Meishan, China

4 Shanxi Aerospace Tsinghua Equipment Co., Ltd, Changzhi, China

proposed that the axial force caused by the transverse edge accounted for 40–60% of the total axial force [2]. Zhang pointed out that the axial cutting force is mainly generated by the horizontal edge and main cutting edge of the drill bit, and its value is affected by many factors such as the geometric size of the tool, processing parameters and processing environment [11]. Hou et al. conducted a hole wall temperature measurement experiment under different fiber cutting angles and different measuring distances and studied the effect of heat accumulation on cutting temperature and damage [12]. Wang et al. analyzed the cutting quality of CFRP unidirectional plates at different temperatures and proved that the high-temperature softening and low-temperature embrittlement characteristics of resin had a direct impact on the cutting performance of CFRP [13]. Xu et al. studied the influence of thermal effects on the material removal mechanism in composite processing and found that the cutting temperature had a great influence on the material removal process [14]. Wang et al. used the reverse cooling process to effectively improve the drilling accuracy by controlling the temperature and support force in the CFRP drilling area [15]. Zhang et al. used the VUMAT subroutine to compile the three-dimensional Hashin failure criterion and material stiffness degradation model and revealed the material removal mechanism in the CFRP high-speed milling process [16]. Chen et al. used COMSOL to establish a numerical model of drilling a unidirectional CFRP temperature field and explored the heat transfer law in the drilling process [17]. The results showed that the temperature field at the outlet had an oval distribution, and the long axis of the ellipse was parallel to the fiber direction. Yang and Li equivalent the heat source of drilling CFRP to a circular plane heat source and established a temperature field model [18, 19]. Bao established a temperature field model by using the conical heat source to simulate the shape of the heat source of the drill tip and verified the effectiveness of the model through experiments [20].

To sum up, experts and scholars have applied numerical models and empirical evidence of change in heat transfer through temperature fields and damage mechanisms in CFRP drilling. Reports confirmed that the thermal patterns influence the CFRP drilling process. To date, a 3D drilling model considering the heat accumulation effect has not been established yet. The damage caused by heat accumulation in CFRP drilling has been lacking. Herein, a simulation model of CFRP drilling considering the heat accumulation effect is established. Considering the normal temperature model and heat accumulation model, the simulation results of drilling axial force and delamination damage are analyzed. The effectiveness of the model is verified by empirical data. The applied model can establish the relationship between machining parameters, drilling axial force, and delamination damage.

2 Three-dimensional drilling simulation model of CFRP considering heat accumulation effect

2.1 Numerical model of temperature field in CFRP drilling

2.1.1 Thermal conductivity of CFRP

The heat conduction characteristics of CFRP show obvious differences in the horizontal and vertical directions, so the homogenization assumption is made in this paper [21]: The fiber and resin are closely bonded, and the contact impedance is ignored. Carbon fibers are uniformly distributed in the resin, and there are no impurities, delamination, or other defects in the preparation. The bonding between layers is tight, and the contact impedance between layers is ignored. Each physical quantity of heat conduction does not change with the change in temperature. Equations (1) and (2) are used to describe the thermal conductivity parameters [21] in the direction perpendicular to the fiber, and the Wiener model [22] is used to estimate the thermal conductivity, as shown in Eqs. (3) and (4).

$$\rho = \rho_f V_f + \rho_r\left(1 - V_f\right) \tag{1}$$

$$c = c_f V_f + c_r(1 - V_f) \tag{2}$$

$$\lambda_{\mathrm{P}}=V_f\lambda_f+(1\text{-}V_f)\lambda_{\mathrm{m}} \tag{3}$$

$$\lambda_{\perp} = \frac{\lambda_f \lambda_m}{V_f\lambda_f+(1\text{-}V_f)\lambda_{\mathrm{m}}} \tag{4}$$

where c_f *and* ρ_f represent the heat capacity and density of carbon fiber respectively; c_r and ρ_r are the heat capacity and density of epoxy resin respectively; c and ρ represent the heat capacity and density of the composite respectively; λ_f and λ_m are the thermal conductivity of carbon fiber and epoxy resin respectively; $\lambda_{//}$ represents the thermal conductivity of the composite material in the direction parallel to the fiber; $\lambda_{\parallel}$ represents the thermal conductivity of the composite in the direction perpendicular to the fiber; and V_f is the volume content of carbon fiber. The thermophysical parameters of unidirectional CFRP are shown in Table 1.

Table 1 Thermophysical parameters of unidirectional CFRP [23]

Parameter	Value
λ_f/(W/(m·K))	10.145
λ_m/(W/(m·K))	0.186
ρ/(kg/m^3)	1600
c/(J/(kg·K))	465
V_f/%	60
$\lambda_{//}$/(W/(m·K))	6.161
$\lambda_{\perp}$/(W/(m·K))	0.282

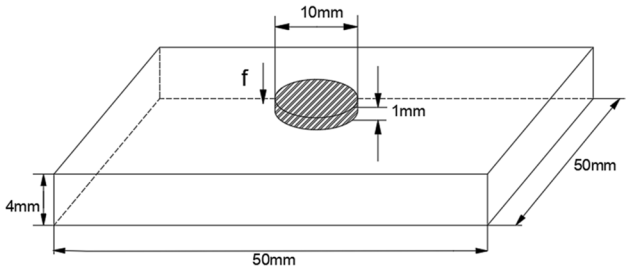

Fig. 2 The model of heat source

2.1.2 Heat source model for CFRP drilling

During the drilling process of a twist drill, the main cutting edge and transverse edge are mainly used to remove the material, while the auxiliary cutting edge is mainly used as a guide. Therefore, the cutting heat during CFRP drilling is mainly generated by the friction between the main cutting edge and the transverse edge with the CFRP, as shown in Q_1 in Fig. 2. The moving speed of the heat source is consistent with the feed speed of the tool. The thickness of the heat source should be less than the projection of the main cutting edge on the spindle [17]. Therefore, the heat source model established in this paper ignores the heat source Q_2 generated by the auxiliary cutting edge and regards Q_1 as a uniform cylinder heat source, as shown in Fig. 1. The thickness of the heat source is taken as half of the projection height of the main cutting edge of the twist drill on the spindle, which is 1 mm. The diameter of the heat source is equal to the diameter of the drill bit, which is 10 mm. Because the heat source only has a great influence on the upper and lower surfaces. Therefore, the upper and lower surfaces of the model are defined as thermal convection boundaries, and the other surfaces are defined as adiabatic surfaces (Fig. 2) .

The instantaneous total heat flow generated by drilling is the sum of shear heat and friction heat, which is expressed by Eq. (5) [24, 25]. It is assumed that the total heat flow generated during drilling is P, the heat flow input to the workpiece is Q_0, and the percentage of heat transferred to the workpiece in the total heat is η. Then, the volume heat flow q [26] transferred to the workpiece per unit volume and unit time can be expressed by the formula:

$$P = Mw + Ff \tag{5}$$

$$q = \frac{Q_0}{V} = \frac{\eta P}{Sh} = \frac{\eta(Mw + Ff)}{\pi(\frac{d}{2})^2 b} \tag{6}$$

where M is torque; w is angular velocity, F is axial force, and f is feed rate; V, S, d, and b are the volume, bottom area, bottom diameter, and thickness of the uniform body heat source, respectively.

2.2 Three-dimensional temperature field simulation model for CFRP drilling

We import the geometric model established above into ABAQUS. The model is meshed by quadrilateral and

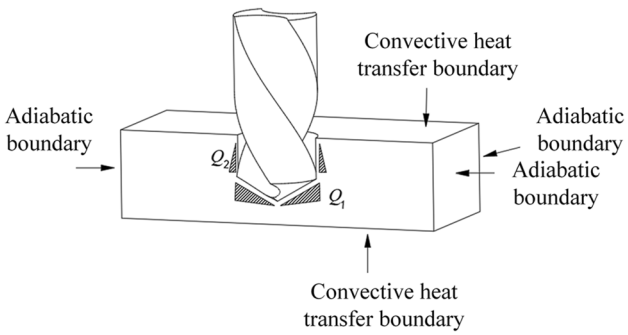

Fig. 1 Boundary conditions of the drilling model

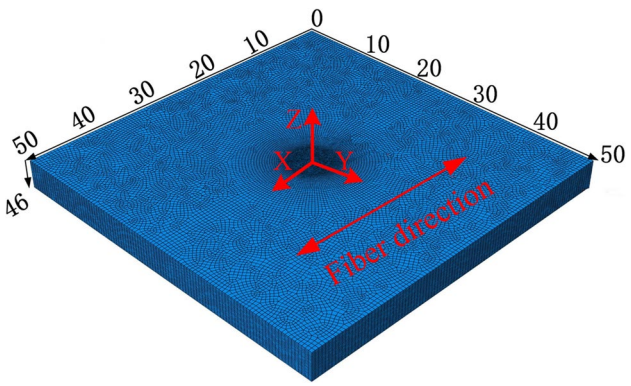

Fig. 3 The diagram of model meshing

Table 2 CFRP material parameters

		298 K (25 °C)	Tg 393 K (120 °C)
Modulus of elasticity/GPa	E_{11}	116	110.69
	E_{22}	8.5	4.11
	E_{33}	8.5	4.11
Poisson ratio	V_{12}	0.02	0.02
	V_{13}	0.02	0.02
	V_{23}	0.28	0.19
Modulus of shearing/GPa	G_{12}	3.26	2.01
	G_{13}	3.26	2.01
	G_{23}	2.12	1.73
Tensile strength/MPa	X_T	1500	1442.64
	Y_T	27	12.18
Compressive strength/MPa	X_C	900	875.86
	Y_C	200	141.81
Shear strength/MPa	S_{12}	80	65.25
	S_{13}	80	65.25
	S_{23}	80	65.25
Density/(kg*m^{-3})	ρ	1580	1580

sweeping, and the DC3D8 element is used as the linear heat transfer element. The grid seeding size is 0.5 mm in the X–Y plane and 0.2 mm in the Z direction. At the same time, in order to improve the calculation accuracy, the grid at the heat source loading position is refined, as shown in Fig. 3. The heat source load is applied by the moving heat source defined by the DFLUX user subroutine, and the flux of the heat source is calculated by Eq. (6). The initial temperature of the workpiece is set at room temperature (13.5 °C), and other boundary conditions are set as shown in Fig. 1.

2.3 Numerical model of CFRP drilling

2.3.1 Constitutive model of CFRP

Carbon fiber-reinforced resin matrix composites are anisotropic [27]. When constructing the constitutive model of materials, it is often simplified as orthotropic materials. Therefore, the stress–strain relationship of CFRP orthotropic material is as follows:

$$\begin{bmatrix}\varepsilon_{11}\\ \varepsilon_{22}\\ \varepsilon_{33}\\ \gamma_{12}\\ \gamma_{13}\\ \gamma_{23}\end{bmatrix}=\begin{bmatrix}\frac{1}{E_1} & \frac{-v_{21}}{E_2} & \frac{-v_{31}}{E_3} & 0 & 0 & 0\\ \frac{-v_{12}}{E_1} & \frac{1}{E_2} & \frac{-v_{32}}{E_3} & 0 & 0 & 0\\ \frac{-v_{13}}{E_1} & \frac{-v_{23}}{E_2} & \frac{1}{E_3} & 0 & 0 & 0\\ 0 & 0 & 0 & \frac{1}{G_{12}} & 0 & 0\\ 0 & 0 & 0 & 0 & \frac{1}{G_{13}} & 0\\ 0 & 0 & 0 & 0 & 0 & \frac{1}{G_{23}}\end{bmatrix}\begin{bmatrix}\sigma_{11}\\ \sigma_{22}\\ \sigma_{33}\\ \tau_{12}\\ \tau_{13}\\ \tau_{23}\end{bmatrix} \tag{7}$$

where ε_{ii} is positive strain; γ_{ij} is shear strain; σ_{ii} is normal stress; τ_{ij} is shear stress; E_i is the elastic modulus; G_{ij} is the shear modulus; and v_{ij} is Poisson's ratio.

2.3.2 Failure criteria for CFRP

The CFRP failure criterion adopts the widely recognized Hashin criterion, which proposes four failure forms [28, 29], namely fiber tensile failure, fiber compression failure, matrix tensile failure, and matrix compression failure.

1) Fiber tensile failure ($\sigma_{11} \geq 0$):

$$F_{ft} = \left(\frac{\sigma_{11}}{X_T}\right)^2 + \left(\frac{\tau_{12}}{S_{12}}\right)^2 + \left(\frac{\tau_{13}}{S_{13}}\right)^2 \tag{8}$$

2) Fiber compression failure ($\sigma_{11} \leq 0$):

$$F_{fc} = \left(\frac{\sigma_{11}}{X_C}\right)^2 \tag{9}$$

3) Tensile failure of the matrix $\left(\sigma_{22} + \sigma_{33} \geq 0\right)$:

$$F_{mt} = \left(\frac{\sigma_{22}+\sigma_{33}}{Y_T}\right)^2 + \left(\frac{\tau_{12}}{S_{23}}\right)^2 - \left(\frac{\sigma_{22}\times\sigma_{33}}{S_{23}^2}\right) + \left(\frac{\tau_{12}^2 - \tau_{13}^2}{S_{13}^2}\right) \tag{10}$$

4) Compression failure of the matrix ($\left(\sigma_{22} + \sigma_{33} < 0\right)$):

$$F_{\mathrm{mc}} = \frac{(\sigma_{22}+\sigma_{33})\times Y_C}{4\times S_{23}^2} - \frac{\sigma_{22}+\sigma_{33}}{Y_C} + \left(\frac{\sigma_{22}+\sigma_{33}}{2S_{23}}\right)^2 + \frac{\tau_{23}^2 - (\sigma_{22}\times\sigma_{33})}{S_{23}^2} + \frac{(\tau_{12}^2+\tau_{13}^2)}{S_{12}^2} \tag{11}$$

In the equation, σ_{ii} and τ_{ij} refer to normal stress and shear stress, respectively; X_T and Y_T represent the tensile strength

Table 3 Tool material parameters

Density	14,500 kg•m^{-3}	**Specific heat**	220 J•(kg•°C)$^{-1}$
Modulus of elasticity	640 GPa	**Thermal conductivity**	75.4 W•(m•°C)$^{-1}$
Poisson ratio	0.22		

along and perpendicular to the fiber direction; X_C and Y_C represent the compressive strength along and perpendicular to the fiber direction; and S_{ij} is the in-plane shear strength.

2.4 CFRP drilling simulation model considering heat accumulation

2.4.1 Physical properties of CFRP based on temperature effect

From the variation of CFRP physical parameters with temperature [14], it can be seen that the physical properties of CFRP components undergo sudden changes within a small temperature range of Tg (120 °C) [12], but as the temperature rise above Tg and continues to rise, the physical parameters of CFRP components tend to stabilize.

Therefore, this article simplifies the physical parameters of CFRP into two types, with specific values shown in Table 2.

2.4.2 *Three-dimensional simulation model for CFRP drilling considering temperature effect*

In the CFRP drilling model, the same carbide twists drill is selected as the tool model. The drilling apex angle is 130°, the helix angle is 30°, and the diameter is 10 mm. The material properties of the drill bit are shown in Table 3. This article only captures the drill bits involved in drilling for grid division, with the grid unit being C3D4 (as shown in Fig. 4), ignoring tool wear and deformation during the simulation process and establishing RP points on the tool model and couple all grid elements of the tool to the RP reference points through rigid body coupling.

Based on the CFRP three-dimensional drilling temperature field model established above, the workpiece model in the

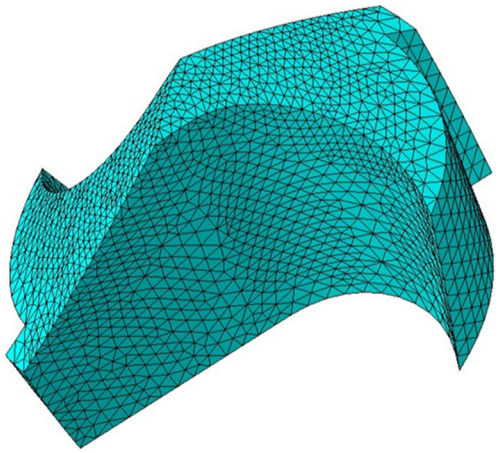

Fig. 4 The diagram of the tool grid division

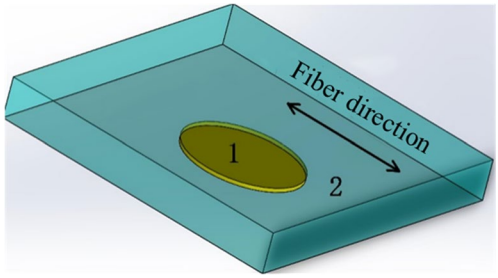

Fig. 5 The model of the workpiece

macro-drilling model is divided into heat accumulation zone 1 and room temperature zone 2, as shown in Fig. 5. Assign zone 1 to the material parameters at temperatures higher than Tg, and assign the remaining parts to the material parameters at room temperature. In order to facilitate the analysis of the effectiveness of the 3D drilling model considering heat accumulation, a room temperature 3D drilling model with identical geometric parameters was established, and the material parameters at room temperature were assigned.

The unidirectional carbon fiber board has 20 layers with a thickness of 0.2 mm. The fiber-laying direction is completed by establishing a local coordinate system. Direction 1 is the fiber direction; direction 2 is perpendicular to the fiber direction; and direction 3 is the ply thickness direction. Different fiber direction angles can be simulated by changing the direction of direction 1 [30]. In order to improve the accuracy of the simulation, the mesh of the machining area is refined during the meshing of the workpiece. The grid cell of the workpiece is set to C3D8R. The stress is transferred between layers through the cohesive element [31], and the specific parameters are described in the literature [32]. The tangent attributes between the contact surfaces are simulated by the penny model, and the normal attributes of the contact are defined by the hard contact model. The friction coefficient between the drill bit and CFRP is 0.15 [33]. Boundary conditions and load settings are shown in Fig. 6.

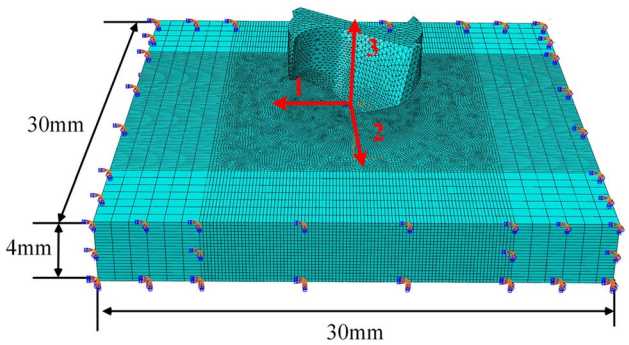

Fig. 6 The model of the drilling simulation

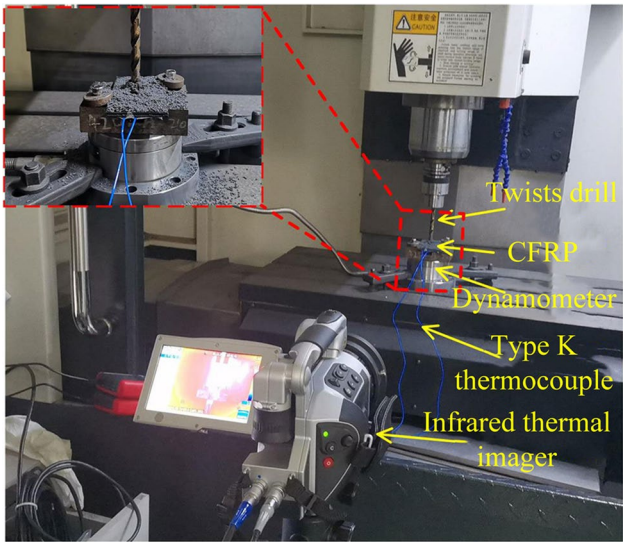

Fig. 7 Schematic diagram of the experimental platform

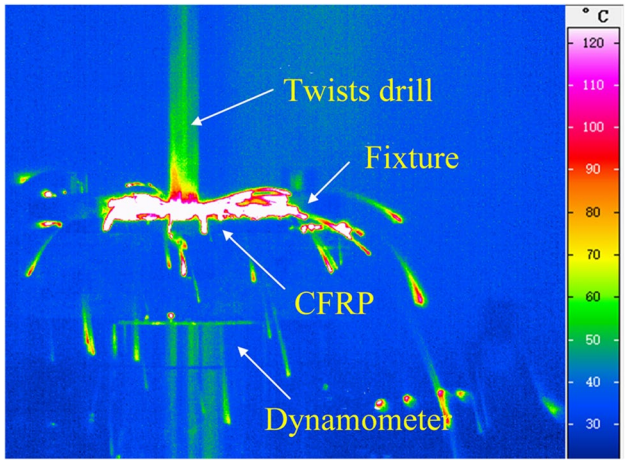

Fig. 9 Thermal image distribution when the transverse edge reaches the exit surface of the workpiece

The above material parameters are substituted into the material failure criterion and damage factor calculation formula, and the VUMAT subroutine written in FORTRAN language is used to realize the three-dimensional drilling damage analysis of CFRP materials.

3 Experimental

3.1 CFRP drilling experiment

In order to accurately obtain the relevant parameters of CFRP drilling, a CFRP dry, unsupported drilling test bed is built in this paper, as shown in Fig. 7. The machine tool used in the experiment is the XK714D CNC vertical milling machine tool of Hanchuan Machine Tool Co., Ltd. The experimental material is unidirectional CFRP made by a molding process; its model is T700/7202 K, and the resin content is 60%. The drilling tool is YG10, and the parameters are as follows: The diameter is 10 mm, the drilling apex angle is 130°, and the helix angle is 30°.

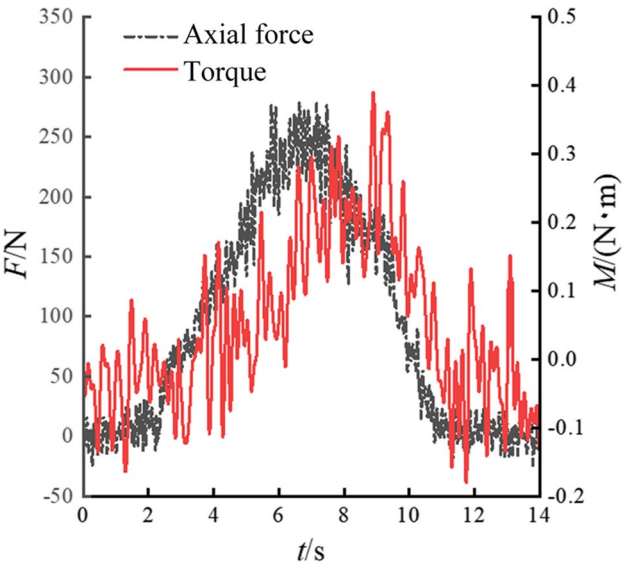

Fig. 8 Axial force and torque in the drilling experiment

The experimental processing parameters are spindle speed 3000 r/min, feed rate 50 mm/min; the experiment is in the room with natural air flow, h = 20 W/(m2·K). The drilling axial force and torque are measured by a Kistler 9272 dynamometer, as shown in Fig. 8. Drilling temperature is measured by the hand-held infrared thermal imager VarioCAM® hr, as shown in Fig. 9. The Ut325 dual-channel K-type thermocouple instrument is used to measure the temperature at the point 1 and 2 (Fig. 10). The measured point is 0.5 mm away from the edge of the machining hole and 0.5 mm away from the exit plane.

3.2 Validation of the temperature field model for CFRP drilling

The value of axial force and torque obtained by empirical data can determine the value of heat source by using Eq. (5). The temperature model was established based on the temperature at the drill tip. It was collected by the thermal imager when the cross edge of the drill bit touched the exit surface of the workpiece. The ratio of the heat transferred into the workpiece to the total heat was 17% under the mentioned processing parameter (Eq. 6). The heat source loading conditions of the CFRP drilling temperature field are listed in Table 4. The drilling temperature field distribution was obtained under the processing parameters.

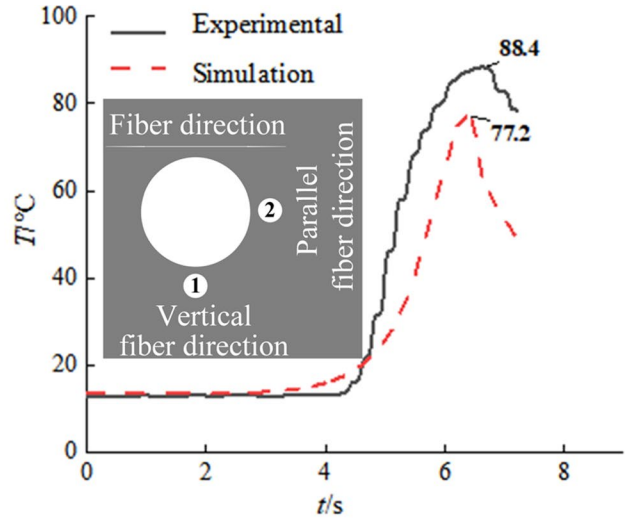

(a) Vertical fiber direction

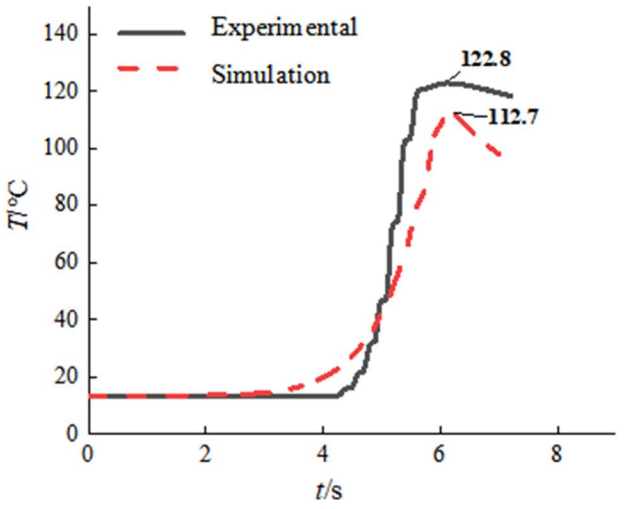

(b) Parallel fiber direction

Fig. 10 a, b Comparison diagram of temperature curve between experiment and simulation

The outcomes of thermocouples were compared with the simulation results of the CFRP temperature field, as shown in Fig. 10. The CFRP temperature field simulation results nearly followed the trend as measured by thermocouple. Particularly, perpendicular to the fiber direction, the maximum simulated temperature is 77.2 °C and the temperature obtained by thermocouple is 88.4 °C. Parallel to the fiber direction, the maximum temperature measured through simulation is 112.7 °C, and the temperature measured by thermocouple is 112.7 °C, i.e., 8.2% error. It confirms that the theoretical approach is consistent with the experiment. The proposed temperature field model can analyze the temperature field of unidirectional CFRP drilling.

From analysis, a slight difference between the simulation and the experimental values is ascribed to the homogenization assumption of the model. The temperature measured by the thermal imager deviates from the real temperature, resulting in altered heat source loading conditions of the temperature field and the real situation. Besides, the temperature measured through thermocouple is slightly high.

Table 4 Parameters of the temperature field model

Parameter	Value
Axial force F/N	225
Torque M/N·m	0.2
Feed rate f/(mm·min^{-1})	50
Angular velocity w/(r·min^{-1})	3000
Convective heat transfer coefficient h/W/(m^2·K)	20
Heat source diameter d/(mm)	10

3.3 Validation of CFRP 3D drilling simulation model considering heat accumulation effect

The mentioned experiments were simulated by using the CFRP 3D drilling model considering heat accumulation and normal temperature effects, and the variation in axial force is shown in Fig. 11. Both applied models show a similar trend in the variation in the axial force as compared to the experimental results. The maximum error between the axial force of heat accumulation model and experimental results is 8.2%. However, the maximum error between the axial force of the normal temperature model and experimental results is 12.9%. Thus, the CFRP 3D drilling simulation model considering heat accumulation effect can precisely analyze and study the impact of axial force in CFRP drilling.

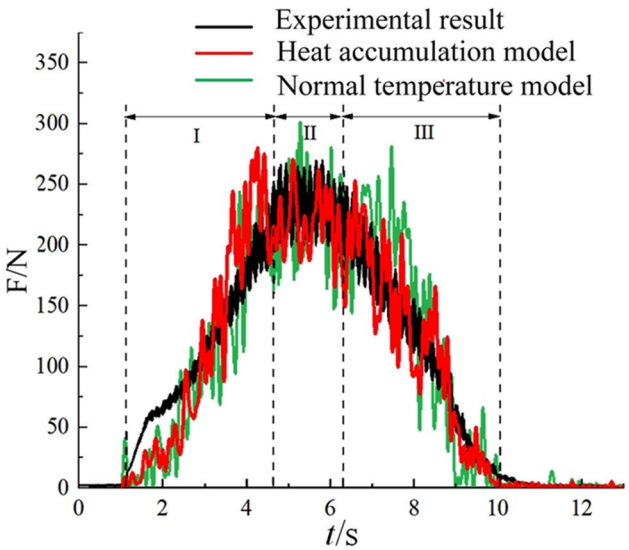

Fig. 11 Comparison of axial force

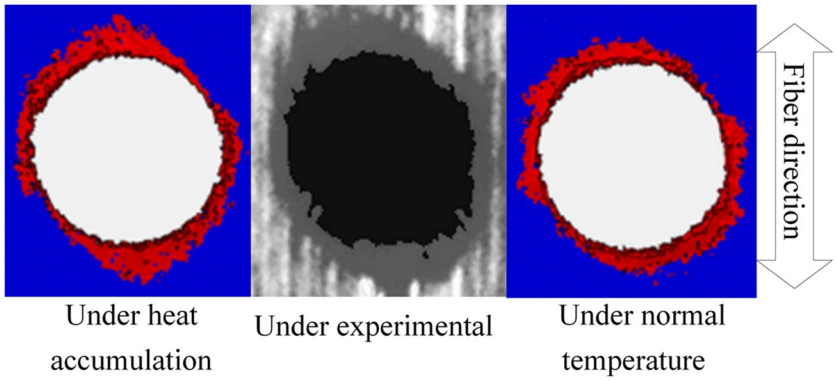

Fig. 12 Delamination damage diagram of CFRP outlet

The high accuracy of the heat accumulation model is attributed to the fact that the heat accumulation model takes into account the changes in material properties caused by heat accumulation during CFRP drilling. At the same time, due to the appropriate simplification of the temperature field model in this paper, there are still some differences between the simulation results and the experimental results of the heat accumulation model.

3.4 Delamination damage verification of the CFRP 3D drilling simulation model considering heat accumulation effect

The water immersion ultrasonic scanning microscope ZS400D was used to detect CFRP outlet, and the images of delamination damage are shown in Fig. 12. Considering the two-dimensional delamination factor [41], the error values of the heat accumulation model and the normal temperature model to the experimental results are 4.6% and 9.8%, respectively. Therefore, the heat accumulation model accurately simulates the delamination damage at the borehole outlet.

The established three-dimensional drilling model of CFRP considering the heat accumulation effect is verified from the aspects of axial force and delamination factor. The specific errors are obtained within the acceptable range. The heat accumulation model precisely depicts the impact and can analyze the drilling characteristics of CFRP than the normal temperature model.

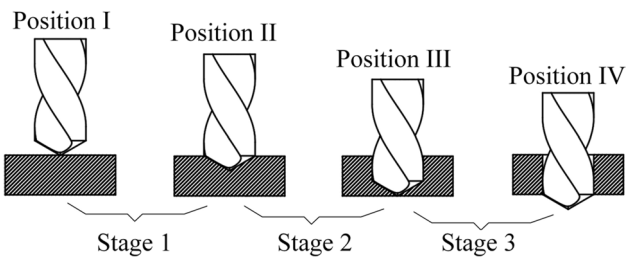

Fig. 13 Schematic diagram of the drilling stage

4 Results and discussion

4.1 Variation law of temperature field at the outlet of CFRP drilling

Combined with the temperature field variation in CFRP drilling process, the process is simplified into three stages, as shown in Fig. 13. Stage 1 is the period from the bit touches the workpiece (position I) to the fully entered main cutting edge of the bit to the workpiece (position II). Stage 2 starts from position II to the period when the transverse edge of the bit just reaches the exit plane of the hole (position III). Stage 3 defines the period when the bit moves from position III to the main cutting edge of the bit leaves the workpiece (position IV).

From the analysis of the above drilling stages, the heat accumulation at stage 1 is the weakest. Stage 2 is semi-enclosed drilling, where heat accumulation continues to increase as the bit penetrates deep, and heat accumulation strengthens as the bit reaches position III. The hole center temperature is 227.5 °C, as shown in Fig. 14 a. In stage 3, as the workpiece is drilled through, the airflow continues to increase, which gradually weakens heat accumulation effect. At position IV, the outlet temperature cloud map is shown in Fig. 14 b, and the heat accumulation effect declines obviously.

The thermal conductivity of carbon fiber bundles along vertical direction is quite different from the parallel direction. The surface temperature of borehole outlet is elliptical at different times. In the drilling process, heat is mainly transmitted by the tool and the workpiece due to the least air circulation in stage 2, resulting in a continuous rise in heat accumulation.

4.2 Evolution of delamination damage at CFRP outlet

For in-depth analysis of the evolution process of delamination damage at the CFRP outlet, drilling stage 3 is divided into two stages: A and B. From Fig. 15, stage A starts when

bit leaves the workpiece from position III to half-length penetration of the bit's main cutting edge (position a). Stage B refers to the drill bit at position "a" to position IV.

As shown in Fig. 15, the bit reaches position III, initiating layer-by-layer damage at the hole outlet, and the damaged area is not completely located in the hole area. This phenomenon is consistent with the reported tear expansion experiment of unidirectional CFRP drilling: the initial crack of the workpiece is not necessarily located in the hole region [10]. By comparing the stratified damage at the exit of the drill bit at position "a" and position IV, the stratified damage range is basically formed when the drill bit reaches position "a," prior to the full penetration of the drill hole. As the bit continues to drill, the bit cuts through excessive material at the exit. The analysis shows that the growth in delamination damage at borehole outlet is consistent with the variation in temperature field at borehole outlet. At position III, the heat accumulation effect is strongest and stratified damage begins to appear. The range of delamination loss is formed during drilling under the effect of heat accumulation and axial force.

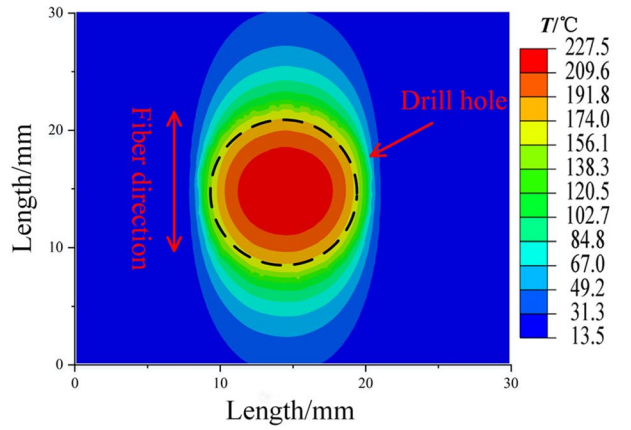

(a) Outlet temperature nephogram at position II

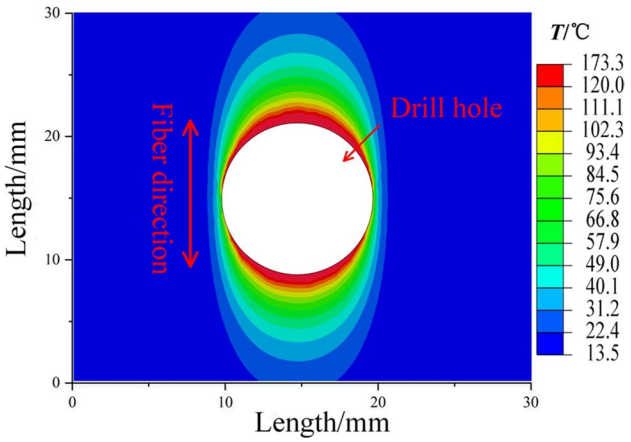

(b) Outlet temperature nephogram at position III

Fig. 14 a, b Outlet surface temperature distribution

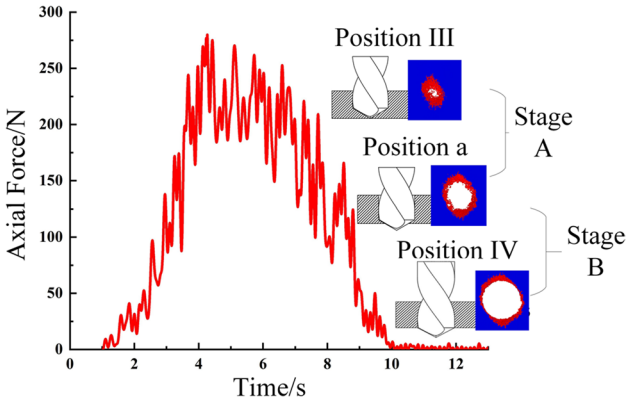

Fig. 15 Axial force and outlet delamination damage in different drilling stages

4.3 Relationship between surface heat accumulation effect and delamination damage in CFRP drilling

To investigate the relationship between the temperature field at the borehole outlet and delamination damage, measure the distance L_1 from the edge of the area (whose temperature is higher than Tg) to the hole center on the outlet temperature nephogram (drill bit at position IV). The whole circumference was measured from 0° fiber cutting angle with a step of 10°. Furthermore, the distance from the layered edge of the workpiece outlet to the hole center (L_2) was measured under the same experimental conditions (Fig. 16). The obtained values of L_1 and L_2 with varying fiber cutting angles are plotted in polar coordinates, as shown in Fig. 17.

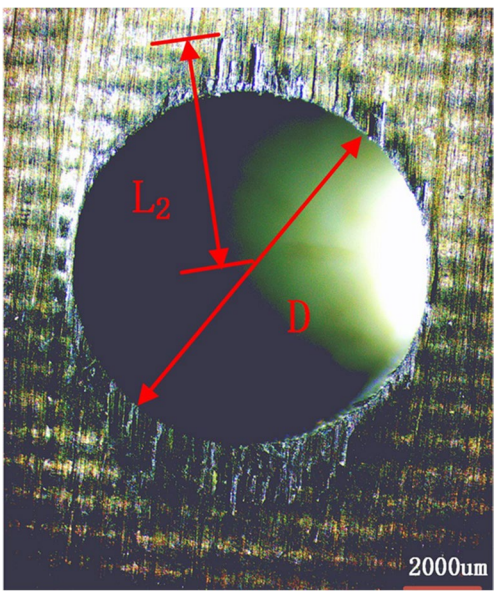

Fig. 16 Delamination damage diagram of CFRP outlet

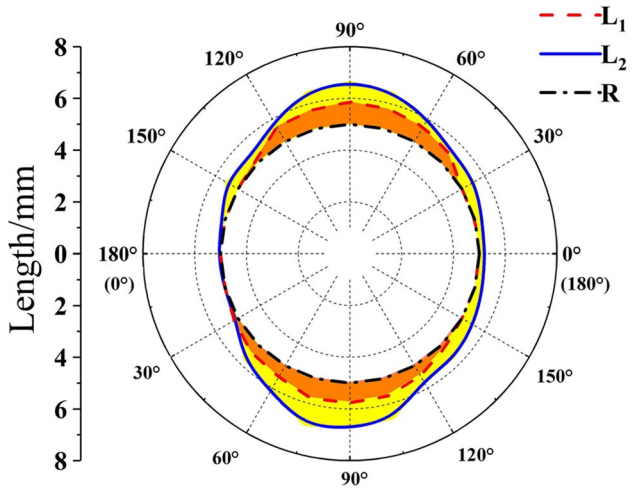

Fig. 17 Changes of L1 and L2 with fiber cutting angle

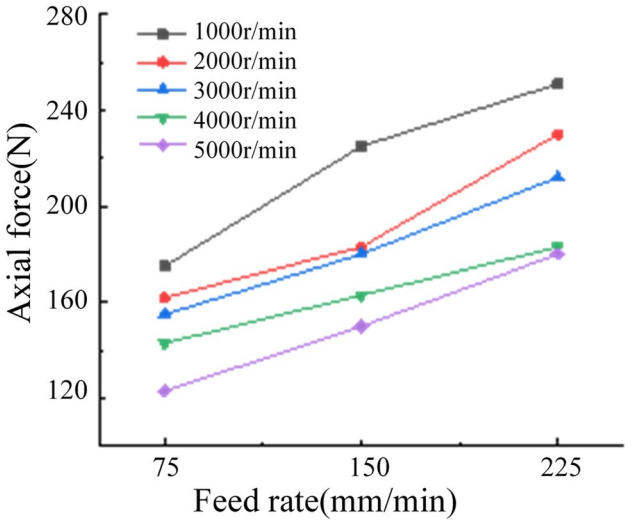

Fig. 18 Variation trend of axial force under different processing parameters

The layered damage profile of the exit is highly consistent with the profile shape of the simulated high-temperature area of the exit surface (Fig. 17). The serious damage occurs around 90° cutting Angle. The outline values of L_1 and L_2 are not exactly consistent. The analysis shows that there are some differences between the temperature model and the actual temperature distribution. Importantly, the edge outline of the CFRP outlet temperature, i.e., outline of L_1 is higher than Tg region (bit at position III). This region exhibits serious heat accumulation, and temperature is higher than Tg for a period in this area.

Considering temperature growth with fiber cutting angle analysis, the delamination damage process of CFRP borehole is closely related to the heat accumulation pattern at the borehole outlet. During the phase of the bit from position III to position "a" (phase—heat accumulation on the surface of the hole outlet is strongest), CFRP hole delamination damage occurred. The damage severity at the hole outlet is positively correlated with the heat accumulation effect and axial force during the drilling bit from position III to position "a."

4.4 Numerical relationship between processing parameters and export delamination damage

Using the established model, the drilling axial force and outlet delamination defects are studied and analyzed under different processing parameters (Table 5). The variation trend of the axial force and delamination factor are shown in Figs. 18 and 19.

Combined with the mentioned analysis, the delamination defect occurs in the phase of the bit from position III to position "a." This stage possesses a high heat accumulation effect, as well as strong drilling axial force. Under certain conditions of machining environment, the axial force and heat accumulation during drilling also depend on machining parameters. The role of machining parameters can cause delamination defects, which can be explained by the impact of machining parameters on the drilling axial force.

Table 5 Processing parameters

Spindle speed (r/min)	Feed rate (mm/min)
1000/2000/3000/4000/5000	75/150/225

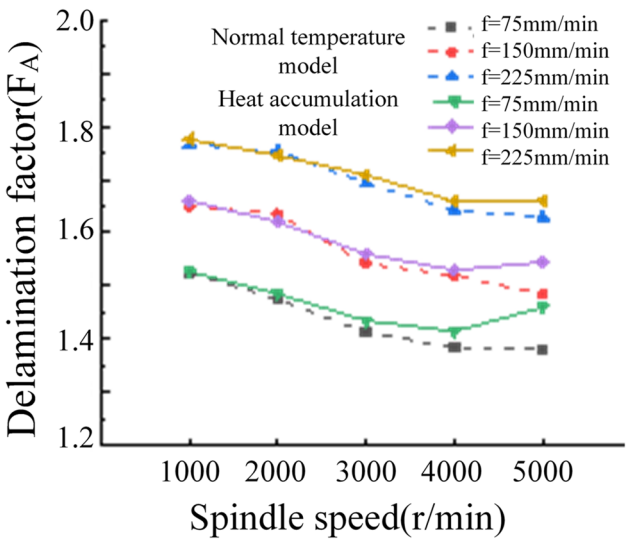

Fig. 19 Variation law of delamination factor of different processing parameters

From previous work [34], an exponential formula is developed to perform multiple regression analysis on the average axial force during the drilling phase. The axial force fitting formula of twist drill for CFRP drilling is expressed as follows:

$$F = 1391 \times \mathrm{n}^{-0.7991} \times f^{0.623} \tag{12}$$

where F is the axial force, N; n is the spindle speed, r/min; and f is the feed rate, mm/min.

At significance level $\alpha = 0.05$, the calculated correlation coefficient $R = 0.901$. $F = 162$ N corresponding probability $P = 0.02 < 0.05$. The regression model was established. At 5000r/min of spindle speed and 150 mm/min of feed rate, the axial force prediction formula shows an error of 10.1%. Thus, the fitting formula can predict the axial force.

The relationship between processing parameters and delamination factor F_A is given as:

$$F_A = 1.78n^{-0.7991} \times f^{0.623} + 1.115 \tag{13}$$

Through the above analysis and research, the quantitative relationship between processing parameters and delamination damage can be explained in a certain processing environment. The quantitative relationship can provide guidance to select processing parameters reasonably during the CFRP drilling process.

5 Conclusions

In summary, a 3D simulation model of CFRP drilling was established to disclose the heat accumulation effect. A CFRP dry drilling experimental platform was built, which validated the model in terms of the surface temperature field distribution of the borehole outlet, the axial force of drilling, and the layering damage of the borehole outlet. The accuracy of the model was proved through comparative analysis of the CFRP 3D drilling simulation model at normal temperature and with heat effect. The surface temperature field and delamination damage of the hole outlet were analyzed during CFRP drilling. The model confirmed that the delamination damage of CFRP unsupported dry drilling occurred when the transverse edge of the bit touched the exit plane of the drilling hole and half of the length of the main cutting edge of the bit penetrated the workpiece. Finally, the model disclosed the variation law of axial force and layering factor under different machining parameters. The quantitative relationship is established between machining parameters and layering factor by multiple regression.

Author contribution All authors contributed to the study conception and design. Experimentation, data collection, simulation, and analysis were performed by YZ, ZH, and GW. The first draft of the manuscript was written by LW, QL, and all authors commented on previous versions of the manuscript. All authors read and approved the final manuscript.

Funding The support of Science and Technology Research Project of Chongqing Education Commission (KJQN202201203) and College Students' Innovative Entrepreneurial Training Plan Program (S202310643004) in carrying out this research are gratefully acknowledged.

Declarations

Conflict of interest The authors declare no competing interests.

References

1. Song X, Pang L (2021) Research advances in molding technology and application of carbon fiber and its resin matrix composites. Packaging Eng 42(14):11. https://doi.org/10.19554/j.cnki.1001-3563.2021.14.009
2. Jain S, Yang D (1994) Delamination-free drilling of composite laminates. J Eng Ind 116(4):475–481. https://doi.org/10.1115/1.2902131
3. Wang F, Qian B, Jia Z, Fu R, Cheng D (2017) Secondary cutting edge wear of one-shot drill bit in drilling CFRP and its impact on hole quality. Composite Structures 178:341–352. https://doi.org/10.1016/j.compstruct.2017.04.024
4. Gulia V, Nargundkar A (2022) Experimental investigations of abrasive water jet machining on hybrid composites. Mater Today: Proc 65:3191–3196. https://doi.org/10.1016/j.matpr.2022.05.372
5. Hejaji A, Singh D, Kubher S, Kalyanasundaram D, Gururaja S (2016) Machining damage in FRPs:laser versus conventional drilling. Compos Part A Appl Sci Manuf 82:42–52. https://doi.org/10.1016/j.compositesa.2015.11.036
6. Salama A, Li L, Mativenga P, Sabli A (2016) High-power picosecond laser drilling/machining of carbon fibre-reinforced polymer (CFRP) composites. Appl Phys A 122(2):1–11. https://doi.org/10.1007/s00339-016-9607-8
7. Ahmad J (2016) Hole quality and damage in drilling carbon/epoxy composites by electrical discharge machining. Mater Manuf Process 31(7):941–950. https://doi.org/10.1080/10426914.2015.1048368
8. Fu R (2017) Research of key technology for low-damage drilling CFRP composites. Dissertation, Dalian University of Technology
9. Dandekar C, Shin Y (2012) Modeling of machining of composite materials: a review. Int J Mach Tools Manuf 57:102–121. https://doi.org/10.1016/j.ijmachtools.2012.01.006
10. Dipaolo G, Kapoor S, DeVor R (1996) An experimental investigation of the crack growth phenomenon for drilling of fiber-reinforced composite materials. J Manuf Sci Eng (No.1):104–110. https://doi.org/10.1115/1.2803629
11. Zhang H (2023) Research on drilling technology of carbon fiber reinforced polymer (CFRP). Dissertation, Beijing University of Aeronautics and Astronautics
12. Hou G, Luo B, Zhang K, Luo Y, Cheng H, Cao S, Li Y (2021) Investigation of high temperature effect on CFRP cutting mechanism based on a temperature controlled orthogonal cutting

experiment. Compos Struct 268:113967. https://doi.org/10.1016/j.compstruct.2021.113967
13. Wang B, Gao H, Wen Q, Wu M, Zhang S (2012) Influence of cutting heat on quality of drilling of carbon/epoxy composites. Mater Manuf Process 27(9):968–972. https://doi.org/10.1080/10426914.2011.610079
14. Xu W, Zhang L (2019) Heat effect on the material removal in the machining of fibre-reinforced polymer composites. Int J Mach Tools Manuf 140:1–11. https://doi.org/10.1016/j.ijmachtools.2019.01.005
15. Wang F, Cheng D, Zhang B, Yan J, Ma J, Wang Z, Wang S (2019) Reversed-air cooling technology for high-quality drilling of CFRP. Appl Compos Mater 26:857–870. https://doi.org/10.1007/s10443-018-9755-4
16. Zhang L, Wang S, Qiao W, Li Z, Wang N, Zhang J, Wang T (2020) High-speed milling of CFRP composites: a progressive damage model of cutting force. Int J Adv Manuf Technol 106:1005–1015. https://doi.org/10.1007/s00170-019-04662-6
17. Chen Y, Li P, Wang C, Qiu X, Li S (2021) Numerical simulation and analysis of temperature field in CFRP drilling. Aerospace Mater Technol 51(02):31–37. https://doi.org/10.12044/j.issn.1007-2330.2021.02.005
18. Yang F, Wang F, Jia Z (2019) Research on temperature field calculation in CFRP/titanium alloy laminated drilling. Electromech Eng 36(12):1261–1265. https://doi.org/10.3969/j.issn.1001-4551.2019.12.005
19. Li J, Zou P, Qiao C, Dong L (2020) Temperature field distribution model in drilling of CFRP/Ti stacks structure. J Phys: Conf Ser 1626(1):12041. https://doi.org/10.1088/1742-6596/1626/1/012041
20. Bao Y, Hao W, Gao H, Liu X, Wang Y (2018) Numerical and experimental investigations on temperature distribution of plain-woven aramid fiber-reinforced plastics composites with low-mild spindle velocities. Int J Adv Manuf Technol 99(1–4):613–622. https://doi.org/10.1007/s00170-018-2424-9
21. Zhu G (2013) Research on drilling temperature field of unidirectional C/E composites. Dissertation, Dalian University of technology
22. Fakhfakh, T, Chaari, F, Walha, L, Abdennadher, M, Abbes, M, Haddar, M (2017) Advances in acoustics and vibration. Proceedings of the International Conference on Acoustics and Vibration (ICAV2016) 21–23. https://doi.org/10.1007/978-3-319-41459-1
23. Zhao Y, Song L, Li J, Jiao Y (2018) Comparison of thermal response mechanism of three-dimensional woven carbon fiber/epoxy resin composites under two measurement methods. J Compos Mater 35(01):103–109. https://doi.org/10.13801/j.cnki.fhclxb.20170322.002
24. Bono M, Ni J (2002) A model for predicting the heat flow into the workpiece in dry drilling. J Manuf Sci Eng 124(4):773–777. https://doi.org/10.1115/1.1511176
25. Denkena B, Maaß P, Schmidt A, Niederwestberg D, Vehmeyer J, Niebuhr C, Gralla P (2018) Thermomechanical deformation of complex workpieces in milling and drilling processes. Thermal Effects Complex Mach Process 1480:219–250. https://doi.org/10.1007/978-3-319-57120-1_11
26. Li H, Song X (2017) Effect of different heat source models on welding temperature field of Q345 medium and heavy plate. Hot Work Technol 46(23):205–209. https://doi.org/10.14158/j.cnki.1001-3814.2017.23.056
27. Shen G, Hu G (1996) Composite mechanics. Tsinghua University Press, Beijing
28. Hashin Z, Rotem A (1973) A fatigue failure criterion for fiber reinforced materials. J Compos Mater 7(4):448–464. https://doi.org/10.1177/002199837300700404
29. Hashin Z (1981) Fatigue failure criteria for unidirectional fiber composites. J Appl Mech 846-852. https://doi.org/10.1115/1.3157744
30. Isbilir O, Ghassemieh E (2013) Numerical investigation of the effects of drill geometry on drilling induced delamination of carbon fiber reinforced composites. Compos Struct 105:126–133. https://doi.org/10.1016/j.compstruct.2013.04.026
31. Yang J (2014) Experimental study on high speed drilling of carbon fiber composites. Dissertation, Hunan University of science and technology
32. Wang G, Melly S (2018) Three-dimensional finite element modeling of drilling CFRP composites using Abaqus/CAE: a review. Int J Adv Manuf Technol 94(1–4):599–614. https://doi.org/10.1007/s00170-017-0754-7
33. Han L, Zhang J, Liu Y, Gu Q, Li Z (2021) Finite element investigation on pretreatment temperature-dependent orthogonal cutting of unidirectional CFRP. Compos Struct 278:114678. https://doi.org/10.1016/j.compstruct.2021.114678
34. Chen M, Xu J, An Q (2019) Cutting theory and application technology of carbon fiber composite and laminated structure. Shanghai Science and Technology Press, Shanghai